(Received 27 April 2026, Accepted 2 June 2026, Scheduled 13 June 2026)

Gain Enhancement and Reduced Isolation of 4-Port Orthogonal Multiple-Input-Multiple-Output Antennas Based on Metamaterial for 5G Applications

Boddapati Naga Prasanna* and Thokala Kalpalatha Reddy

Department of ECE, Dr. M. G. R. Educational and Research Institute, Chennai 600095, Tamil Nadu, India

ABSTRACT: As the need for rapid data transmission and dependable wireless networks grows, so does the need for advanced antenna technology. This has become a major focus of modern communication technologies. This paper describes the design of a 4-port multiple-input multiple-output (MIMO) microstrip patch working at 28 GHz in the Ka-band. This antenna is fabricated on a substrate measuring $21 \times 21 \times 3.97\,\text{mm}^3$, composed of FR4, foam, and RT/Duroid 5880. It uses a microstrip feed. Performance enhancements are achieved by positioning the feeds orthogonally, incorporating a U-shaped slot into the MIMO antennas, and implementing a metamaterial (MTM) superstrate. Additionally, a single-layer MTM superstrate with rectangular slots is created to improve gain while keeping good impedance matching. The design process systematically improves gain and mutual coupling while keeping the overall size compact. The specific challenge addressed by the design is to improve peak gain and radiation efficiency by employing MTM elements operating at 28 GHz. The 4-port MIMO antenna achieves an impedance bandwidth (IB) of 27.11–29.21 GHz, with a peak gain of 14.5 dB, respectively. This antenna is used in next-generation communication systems, vehicular networks, and 5G systems.

1. INTRODUCTION

As wireless communication devices continue to advance, there will always be a need for small, efficient antennas to support high data rates, improve connection stability, and optimize bandwidth usage [1]. Mobile MIMO antennas have changed the game by increasing the number of channels, changing their locations, and improving signal quality [2]. Due to its small size and simple assembly, the microstrip antenna (MA) has been the go-to choice for MIMO deployments [3, 4]. Metamaterials (MTMs) are included in MIMO systems and can be employed at Ka-band frequencies to increase gain and reduce separation. The primary purpose of the study is to optimize gain and port separation for a 4-port MIMO system. This ensures that high-speed communication functions reliably across a broad frequency range. MTM models can raise MIMO system performance and signal attenuation when suitably designed. There are various applications of metamaterials, which are artificial materials with electromagnetic properties not found in nature. Two of them have a negative refractive index and can stop electromagnetic waves. This has an immediate effect, improving antenna performance [5]. Their unique properties can be used to boost radiation efficiency by preventing adjacent antenna components from coming into contact. In [6–9], isolation enhancement had been achieved by employing MTM, defective ground structure (DGS), and stub loading for mm-wave and the Internet of Things (IoT) applications. Swetha et al. [10] designed a MIMO antenna by integrating orthogonal diversity, a DGS, and parasitic elements, achieving improved isolation and gain without significantly increasing overall dimensions. Elahi et al. [11] employed mode diversity to isolate MA arrays. This design was employed to reduce mutual coupling without using decoupling structures, unlike traditional designs that excited comparable modes in each MIMO array element. Srivastava et al. [12] developed a 16-port MIMO MA for sub-6 GHz communication systems, using 8 dual-polarised elements in a 2×4 array configuration. The design improved the compactness and efficiency of antenna systems for modern communication technologies. Wang et al. [13] constructed and tested a lightweight L-band aperture-coupled MA array for spaceborne synthetic aperture radar. By combining the radiating patch and aperture-coupling layer into a membrane layer, the aperture-coupled antenna was lighter and smaller than traditional designs. Wong et al. [14] described a mobile 16-port MIMO antenna module. The design contains a 16-port MIMO module array supporting 8 spatial streams and 16 receiving antennas across 7.025–8.4 GHz. An ultra-compact DGS 4-port MIMO system for 28/38 GHz was designed by Elabd and Al-Gburi [15]. Devana et al. suggested a compatible antenna covering key 5G bands, as it operates over a broad sub-6 GHz range [16]. In [17–21], a gain improvement and better isolation were achieved for the MIMO antenna using MTM for mm-wave applications. Table 1 shows that most MIMO antenna designs employ complex arrangements, such as coaxial feeding structures, shielded cavities, and dual-polarised elements. They boost performance but require sophisticated fabrication and greater costs.

* Corresponding author: Boddapati Naga Prasanna (prasannavamsi4@gmail.com).

TABLE 1. Comparison of the proposed work with the literature survey.

Ref. No.	Volume (mm^3)	Patch shape	Substrate	MIMO layout	Dielectric layers
[11]	$50 \times 41.5 \times 1.524$	Various-sized rectangles	RogersRO4003C	1×4	1
[12]	$88 \times 44 \times 0.508$	Square with slots	RT/Duroid 5880	2×4	1
[13]	$150 \times 120 \times 58$	Rectangle with slots	Polyimide	4×4	1
[14]	$40 \times 40 \times 0.9$	Square with slots	FR4	4×4	1
[15]	$17.76 \times 17.76 \times 1.52$	Rectangle with slots	Rogers TMM4	2×2	1
[16]	$46 \times 46.5 \times 0.6$	Nested rings	Polyimide	2×2	1
Proposed	$21 \times 21 \times 3.97$	Rectangle with U-slots	FR4, RT/Duroid 5880	2×2	2

The objective of the research is to develop a MIMO system that is both simple and highly effective, utilizing U-shaped slot MIMO antennas loaded with MTM elements that resonate at 28 GHz, corresponding to the Ka band. Consequently, MIMO MAs for these 5G applications provide compact, high gain, and negligible mutual coupling. These conditions are met in this design through a straightforward configuration that primarily focuses on increasing antenna isolation, thereby improving peak gain performance. The research is organized as follows. Section 2 represents the U-shaped MIMO system and its evolution. Section 3 presents the performance of an MTM-based MIMO system. Section 4 explains the MIMO characteristics.

2. U-SHAPED MIMO DESIGN & ITS EVOLUTION

The MIMO antenna shown is based on a rectangular microstrip patch arrangement. This setup is flat, can emit high-frequency radiation, and is easy to integrate. The MIMO antenna initially resonates at 28 GHz, a frequency in the Ka-band spectrum commonly used for satellite communication. Later, to achieve perfect impedance matching, a U slot is initiated into the MIMO system, which resonates at 28 GHz, a frequency in the Ka-band used for 5G and future wireless applications. The considered MA is fabricated on a 0.8 mm FR4 substrate with an ε_r of 4.4 and a dielectric loss ($\tan\delta$) of 0.02. This is to keep the surface waves from spreading and to keep the MA compact. The FR4 substrate was chosen because it is inexpensive and performs well in the Ka-band. In this section, we will show how the proposed antenna was systematically designed and how geometric factors, including impedance matching, bandwidth, and mutual coupling, affect its electromagnetic performance. The suggested MIMO system can be implemented using the equations shown below [22]. The fundamental configuration, as depicted in Fig. 1(a), comprises a rectangular radiating 1×2 patch (A#1) that is excited through a microstrip feed line.

$$W_P = \frac{c}{2f_r}\sqrt{\frac{2}{\varepsilon_r + 1}} \tag{1}$$

$$L_P = \frac{\lambda_g}{2} - 2\Delta L \tag{2}$$

Figure 1(b) illustrates the proposed MIMO antenna (A#2) with U-shaped slots. The supply lines are designed to excite

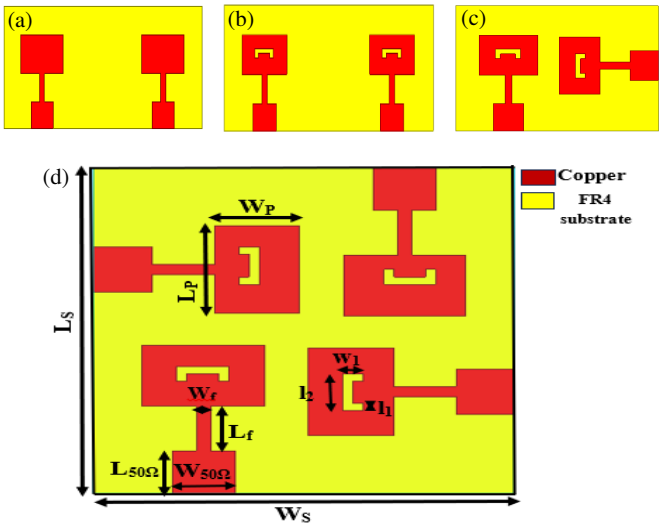

FIGURE 1. (a) Patch separation with $\lambda/2$ spacing (A#1), (b) U-shaped patch separation with $\lambda/2$ spacing (A#2), (c) 1×2 orthogonally placed MIMO (A#3), and (d) 2×2 orthogonally placed MIMO (A#4).

the fundamental TM_{10} mode by optimizing impedance matching (50 Ω). One of the fundamental design issues in MIMO systems is ensuring sufficient spatial separation and isolation among MAs to reduce mutual coupling. To make the antenna smaller while keeping the MIMO elements separate, they are kept $\lambda/2$ apart from adjacent elements. The resonant frequency of the antenna depicted in Fig. 1(a) is 28 GHz, corresponding to a wavelength of $\lambda = 107$ mm. A#1 takes up more space because of the $\lambda/2$ gap. To achieve better impedance matching, U-shaped slots are etched on A#1, which operates at Ka-band (A#2), as shown in Fig. 1(b). Here, 1×2 MIMO elements (A#3) are aligned orthogonally to reduce mutual coupling, as seen in Fig. 1(c). Later, symmetric 2×2 MIMO elements (A#4) aligned orthogonally to reduce mutual coupling, as seen in Fig. 1(d).

Figures 2(a)–2(b) display the fabricated prototypes of the 4-port MIMO system. The surface current density of the suggested MIMO antenna with each port excitation is represented in Figs. 3(a)–3(d). From the simulation output, it is clear that the surface current is effectively confined around the active port, whereas the other ports exhibit very low surface current density. This indicates that there is indeed isolation of each port and therefore individual operation. Fig. 4(a) displays the

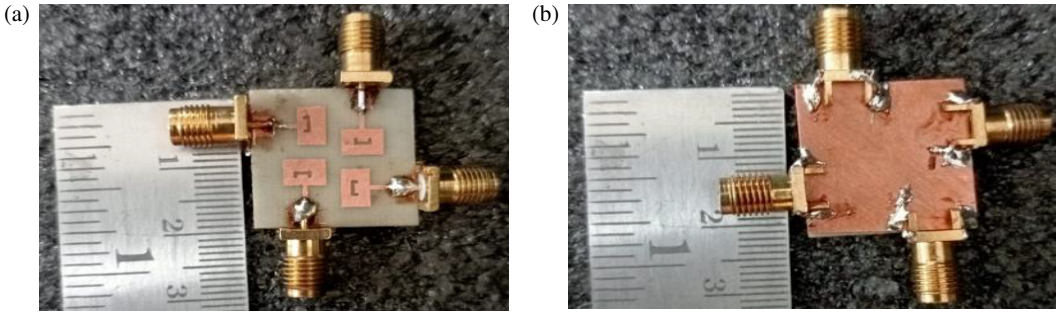

FIGURE 2. Fabricated model of a MIMO system (A#4). (a) Front view and (b) Back view.

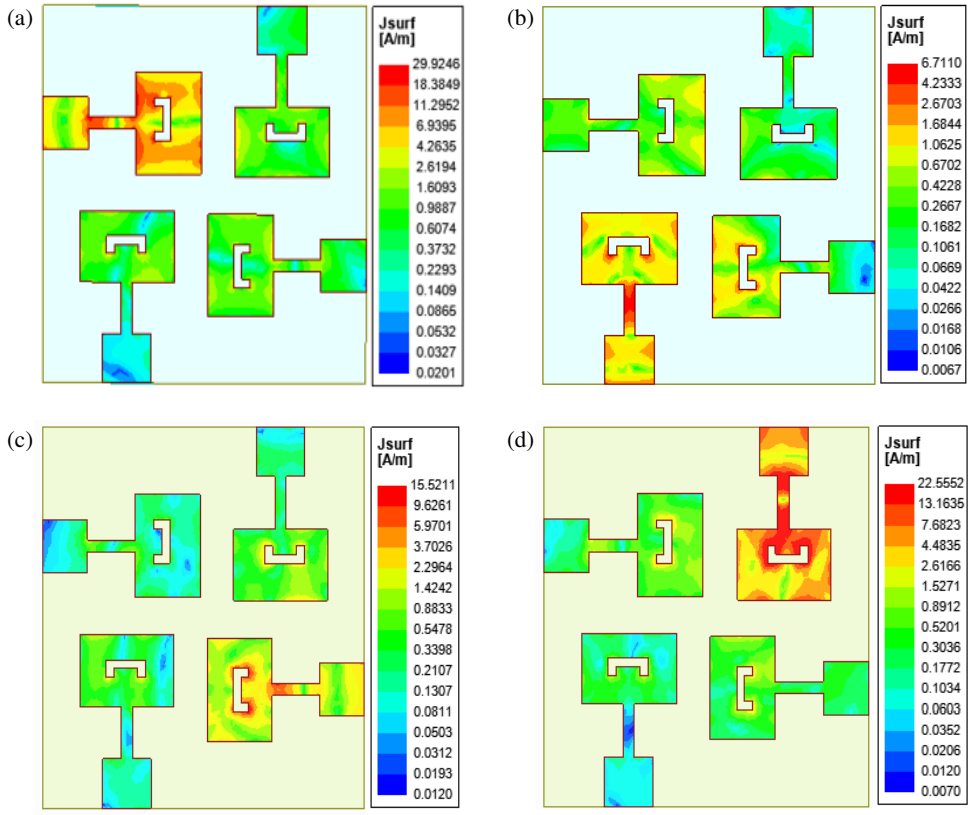

FIGURE 3. Surface current density of the suggested MAs across all the ports. (a) Port-1, (b) port-2, (c) port-3, and (d) port-4.

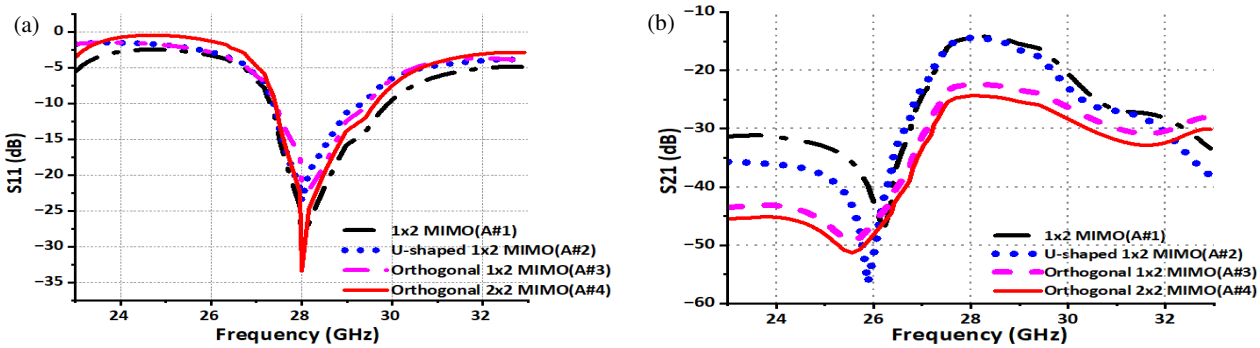

FIGURE 4. (a) S_{11} (dB) and (b) S_{21} (dB) values of all MIMO systems.

TABLE 2. The variables and values of A#4.

Variables	W_S	L_S	L_P	W_P	L_f	W_f	$W_{50\,\Omega}$	$L_{50\,\Omega}$	h_1	w_1	l_1	l_2
Value (mm)	21	21	3.2	2.68	1.9	0.7	1.49	2.83	0.8	0.4	0.2	0.8

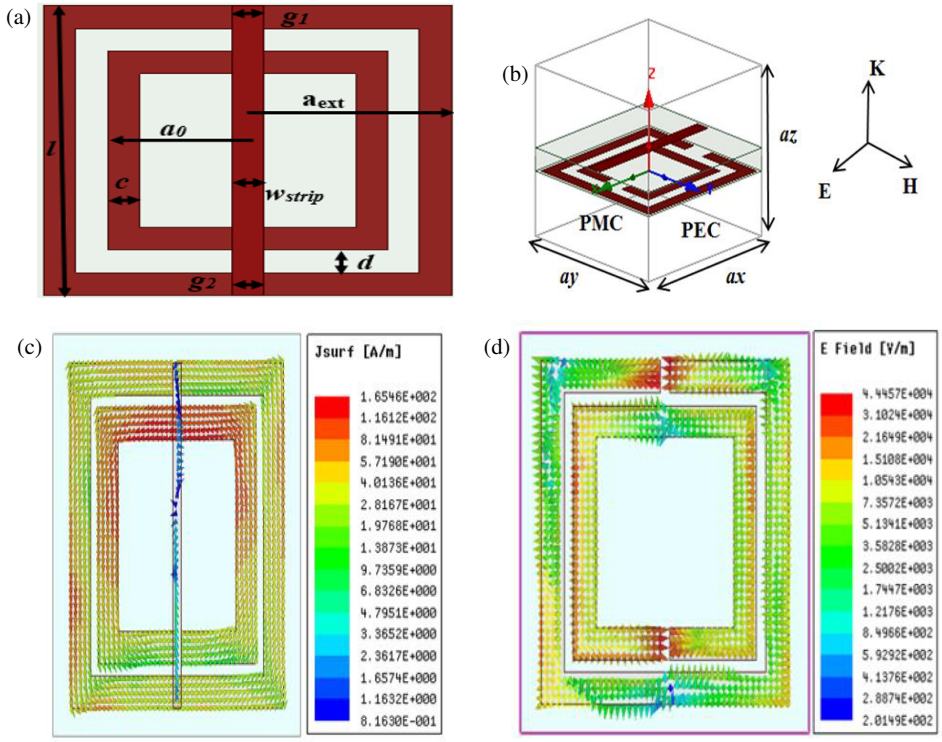

FIGURE 5. (a) MTM segment, (b) Floquet Port, (FP) of MTM, (c) surface current, and (d) E at 28 GHz.

S_{11} of all the antennas A#1–A#4 with their return loss values at 28 GHz. The S_{11} value for the suggested A#4 at 28 GHz is -33.38 dB, as depicted in Fig. 4(a). Fig. 4(b) illustrates the S_{21} value, a measure of port isolation. An orthogonal alignment maintains a strong isolation response, with S_{21} values always below -24.26 dB over 27.11–29.21 GHz. These findings highlight the importance of achieving maximum impedance matching (S_{11}) and effective inter-element isolation (S_{21}). This is critical for MIMO systems to function well across a wide range of frequencies. Table 2 presents the dimensions of the antenna model under consideration. It comprises a patch, a substrate, a feed, and U-shaped slots with sizes for both the single-element patch and the 4-port MIMO system.

3. PERFORMANCE OF THE MIMO SYSTEM BASED ON MTM

In this section, 4×4 MTM cells are added to the MIMO system from the previous part to improve its radiation performance. An artificial dielectric superstrate is used to increase the radiated power density (RPD) of MIMO systems. The MTM layer enhances the spatial fields and enlarges the broadside RPD of the MIMO system. It is also important to note that increasing the unit cell inductance is the best way to reduce the structure's electrical resonance and align it with the resonant frequency of a MIMO system. Fig. 5(a) shows the suggested structure for the unit cell. Here $a_{\text{ext}} = 2.55$ mm, $a_0 = 1.75$ mm, $c = 0.4$ mm, $d = 0.4$ mm, $g_1 = 0.2$ mm, and $g_2 = 0.2$ mm are depicted in Fig. 5(a). The MTM is printed on an RT/Duroid material, 0.8 mm thick, with an ε_r of 2.2. Fig. 5(b) shows the configuration for the unit-cell simulation, with $a_x = a_y = a_z = 3.8$ mm. A VBScript file in High Frequency Structure Simulator (HFSS) uses Eqs. (3)–(12) [23] to find the values of permittivity and permeability.

$$\mu = \eta \times z \quad \text{and} \quad \varepsilon = \frac{\eta}{z} \tag{3}$$

where,

$$\eta = \frac{1}{kd}\cos^{-1}\left[\frac{1}{2S_{21}}\left(1 - S_{11}^2 + S_{21}^2\right)\right]$$

$$\text{and} \quad z = \sqrt{\frac{(1+S_{11})^2 - S_{21}^2}{(1-S_{11})^2 - S_{21}^2}} \tag{4}$$

The frequency f_0 of a single MTM is

$$f_0 = \frac{1}{2\pi}\sqrt{\frac{1}{L_T C_{eq}}} \tag{5}$$

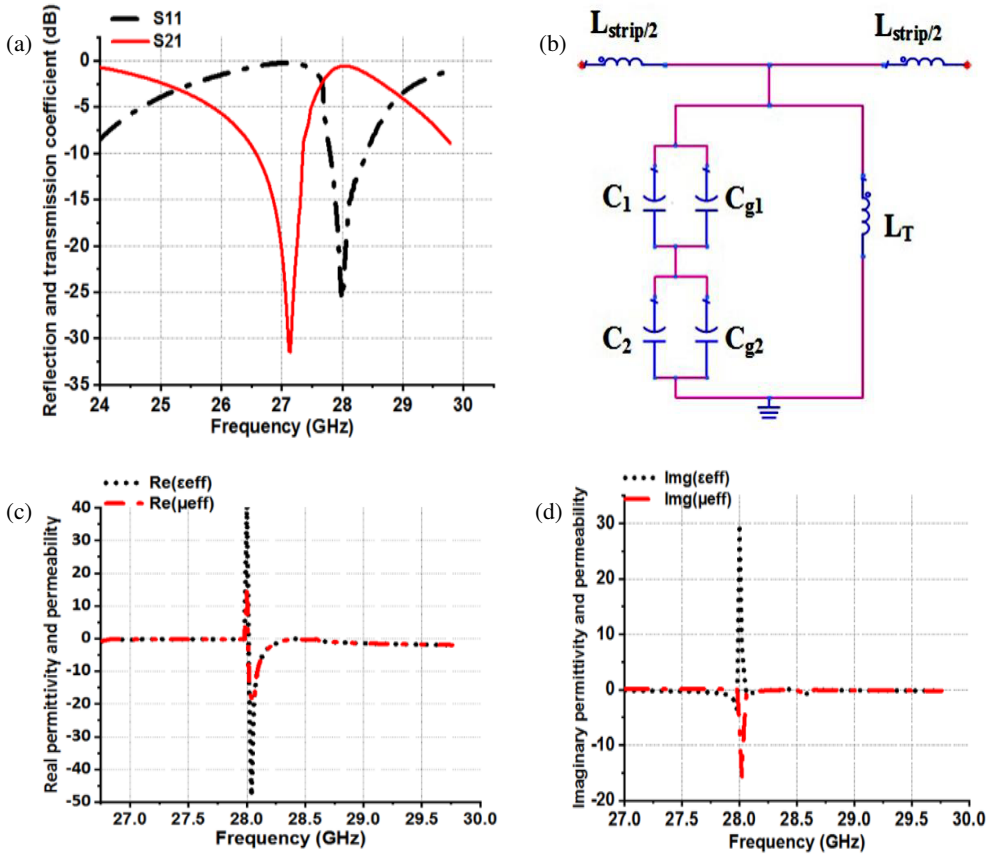

FIGURE 6. (a) S_{11} and S_{21}, (b) equivalent circuit of an MTM, (c), (d) real and imaginary values of ε_{eff} and μ_{eff} at 28 GHz.

where,

$$C_{eq} = \frac{(C_1 + C_{g1})(C_2 + C_{g2})}{(C_1 + C_{g1}) + (C_2 + C_{g2})} \tag{6}$$

Although the split gaps have the same $g_1 = g_2 = g$, values, the gap capacitances $C_{g1} = C_{g2} = C_g$ and the series capacitances $C_1 = C_2 = C_0$ are also the same, and thus Eq. (6) is revised as,

$$C_{eq} = \frac{(C_0 + C_g)}{2} \tag{7}$$

By assigning a metal thickness, t of the strip conductors, the gap capacitances C_{g1} and C_{g2} can be represented as

$$C_{g1} = C_{g2} = C_g = \frac{\varepsilon_0 ct}{g} \tag{8}$$

where c and t are the width and thickness of the metallic rings, respectively. The average ring dimension is given by,

$$C_0 = C_1 = C_2 = (4a_{avg} - g)\, C_{pul} \tag{9}$$

where,

$$a_{avg} = a_{ext} - c - \frac{d}{2} \quad \text{and} \quad C_{pul} = \frac{\sqrt{\varepsilon_e}}{c_0 Z_0} \tag{10}$$

$$L_T = 0.0002 l_1 \left(2.303 \log_{10} \frac{4l_1}{c} - \gamma\right) \mu\text{H} \tag{11}$$

$$\gamma = 2.853 \quad \text{for a wire, and} \quad l_1 = 8a_{ext} - g \tag{12}$$

The calculated MTM values are $L_T = 2.764$ nH, $C_{eq} = 0.01096$ pF, and $f_0 = 28.01$ GHz. The current curve shows the inductance of the copper ring (L_T) and the strip (L_{strip}) in Fig. 5(c). The E plot shows the distributed capacitances C_1 and C_2 and the gap capacitances C_{g1} and C_{g2}, as depicted in Fig. 5(d). To obtain μ and ε of MTM, initially assign the FP study to display the S values indicated in Fig. 6(a). The equivalent circuit of an MTM element is shown in Fig. 6(b). Using the parameter retrieval procedure on an MTM predicated on the Nicholson-Ross-Weir (NRW) approach [23], we obtained the values of μ_{eff} and ε_{eff}, which are shown in Figs. 6(c) and 6(d). At 28 GHz, we found peak values of ε and μ of 40 and 15.5, which are consistent with the configuration's resonance. Here, A#4, equipped with a superstrate of 16 MTM elements, has its S_{11} and S_{21} values indicated in Figs. 7(a)–7(d) within an anechoic chamber test setup.

Figures 7(e)–7(f) present the S-parameter results, showing good S_{11} and isolation characteristics across the working band, with return loss below -26 dB and isolation better than 22 dB. The measured S_{11} tilted in terms of resonating frequency from 28 GHz to 28.14 GHz due to slitting in 4 feeds.

Figures 8(a) and 8(b) show the RPs in the E ($\phi = 0°$) and H ($\phi = 90°$) planes of the orthogonal 2×2 MIMO system (A#4) and the recommended A#4 with a superstrate of 16 MTM elements (A#5) working at 28 GHz. The pattern identifies a

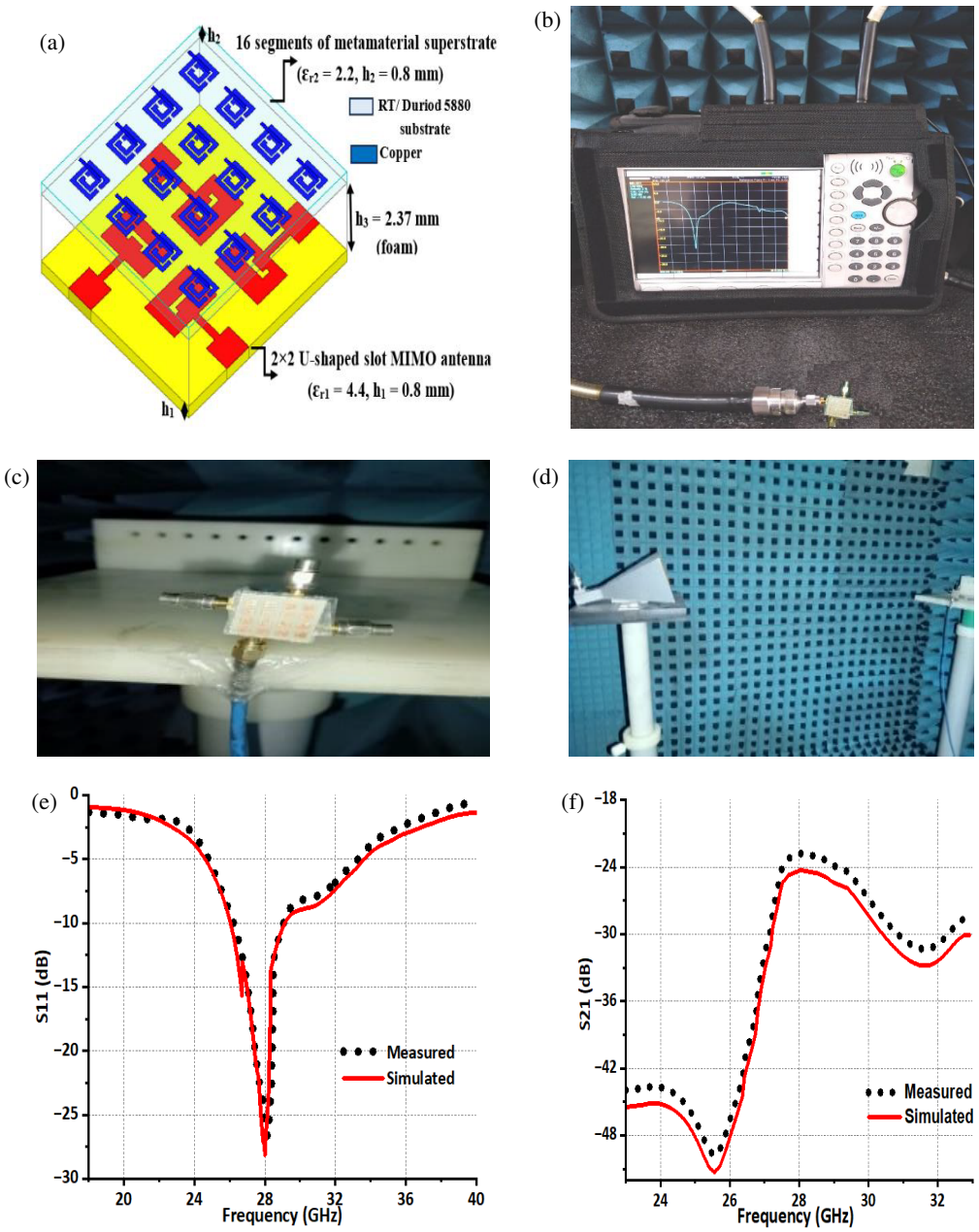

FIGURE 7. (a) MIMO antenna with 16 MTM segments (A#5), (b)–(d) test setup in an anechoic chamber, (e)–(f) measured S_{11} & S_{21} values of MIMO antenna with 16 MTM segments (A#5).

Co-Pol gain of 14.05 dBi and 14.06 dBi in the E & H-plane, respectively, at 28 GHz. Figs. 9(a) and 9(b) show the top and bottom views of the recommended antenna with a 16-MTM superstrate. By employing 16 MTM elements above the MIMO antenna, the peak gain and radiation efficiency (RE) of A#4 and A#5 increased from 7.9 dBi to 14.05 dBi and from 76.14% to 95.46%, respectively, as indicated in Fig. 10(a) and Fig. 10(b).

4. MIMO CHARACTERISTICS

A MIMO antenna is evaluated using different MIMO parameters to assess multiple factors. These parameters include Total Active Reflection Coefficient (TARC), Diversity Gain (DG), Channel Capacity Loss (CCL), and Envelope Correlation Coefficient (ECC).

$$\text{TARC} = \sqrt{\frac{\sum_{x,\,y=1}^{p} |S(x,\,y)|^2}{2}} \tag{13}$$

$$\text{DG} = 10\sqrt{1 - \text{ECC}^2} \tag{14}$$

$$\text{ECC} = \frac{\left| \oint\!\!\oint_{4\pi} \left(\vec{F}_1(\theta,\varphi) \cdot \vec{F}_2^{*}(\theta,\varphi) \right) d\Omega \right|^2}{\oint\!\!\oint_{4\pi} \left| \vec{F}_1(\theta,\varphi) \right|^2 d\Omega \oint\!\!\oint_{4\pi} \left| \vec{F}_2(\theta,\varphi) \right|^2 d\Omega} \tag{15}$$

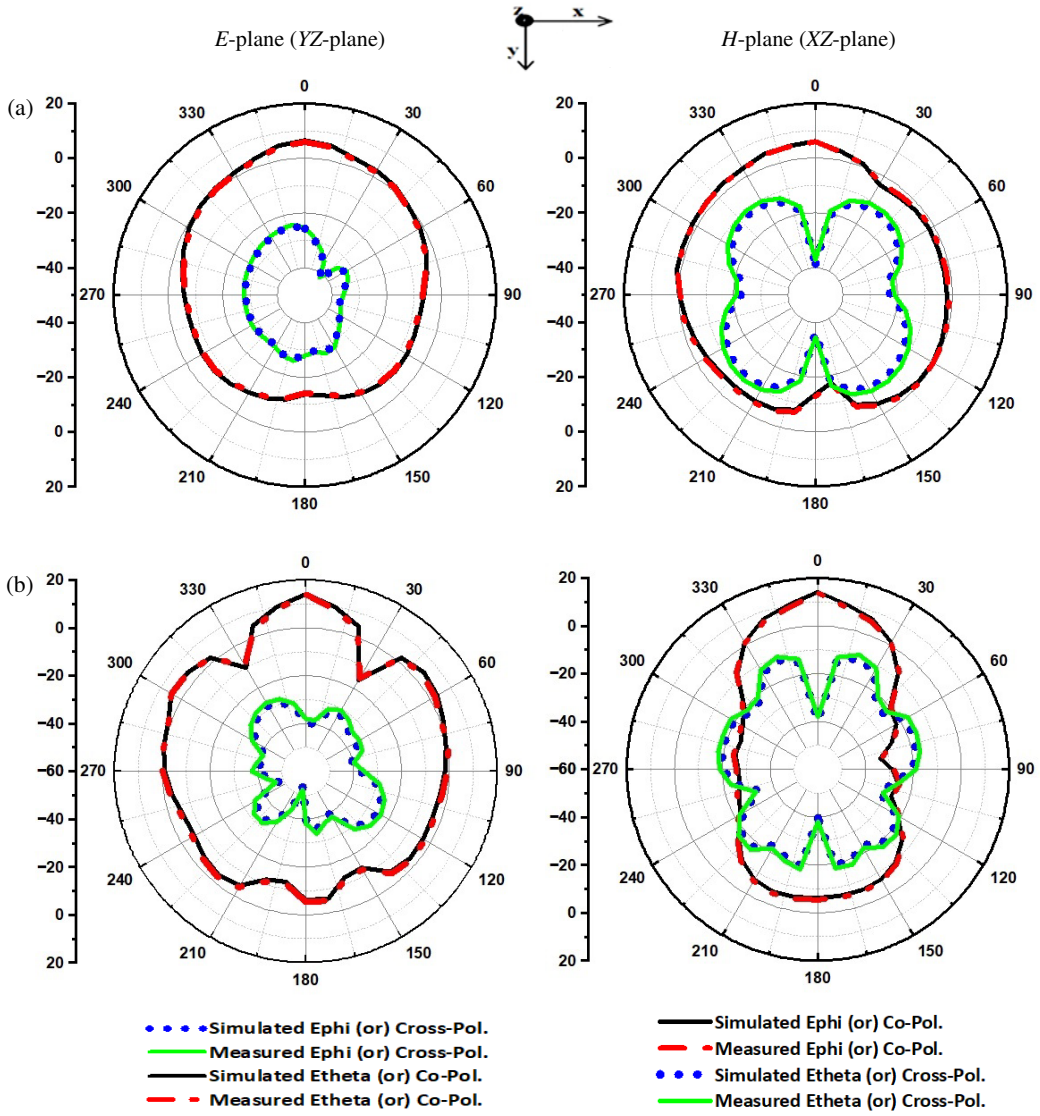

FIGURE 8. Measured radiation patterns (RP) of (a) MIMO system (A#4), and (b) MIMO system loaded with MTM superstrate at 28 GHz (A#5).

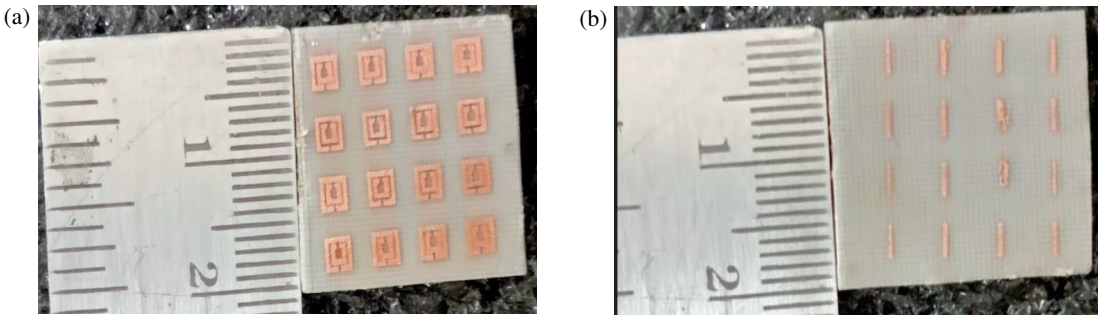

FIGURE 9. (a) Bottom view and (b) top view of the A#5.

$$\text{CCL} = -\sum_{x=1}^{p} \log_2\left(1 - |CC_x|^2\right) \tag{16}$$

where Eqs. (13) to (16) represent TARC, DG, ECC, and CCL, respectively. Here, p denotes the overall ports; $S(\cdot,\cdot)$ signifies the S-parameters; *conjg* represents the complex conjugate; and CC represents the correlation coefficient of the xth antenna element. When MIMO antenna systems are used, TARC is utilized to measure the complete return loss of an antenna array. A best TARC (< -10 dB) indicates that the antenna is good at radiating power rather than reflecting it to the transmitter, which improves performance. The TARC value also shows how well the MIMO elements (various patch topologies) in a MIMO antenna work together. Fig. 11(a) shows that all ports are active,

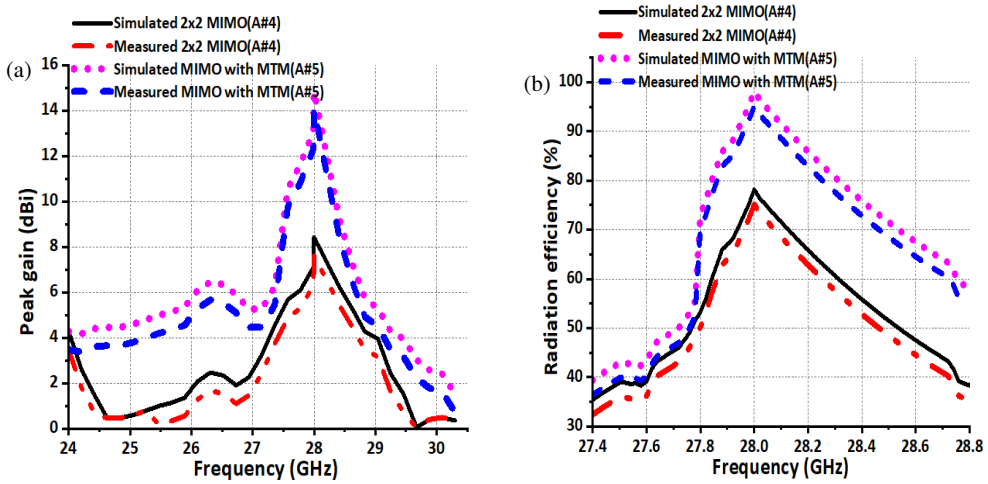

FIGURE 10. (a) Peak gain and (b) radiation efficiency (RE) of A#4 and A#5.

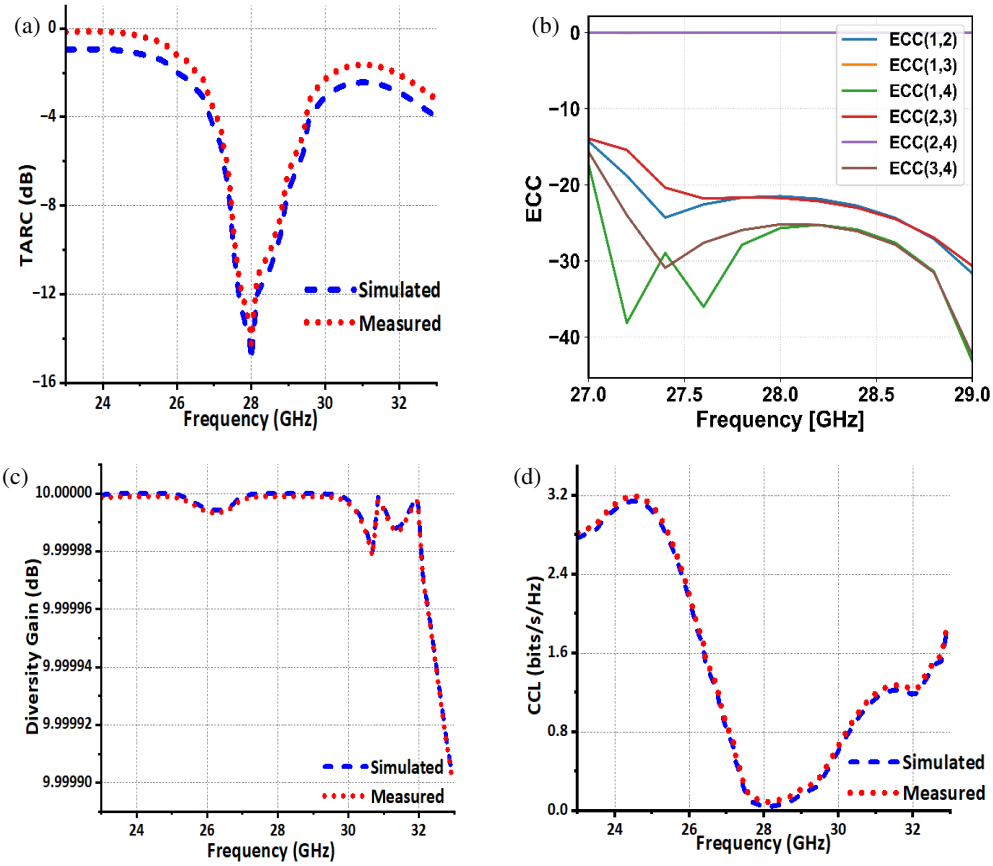

FIGURE 11. (a) TARC, (b) ECC, (c) DG, and (d) CCL of the A#5.

with better isolation below −21 dB and little reflection, which is very important for real-world MIMO arrangements.

ECC is an important parameter for describing the relationship between antennas. Here, ECC is considered in terms of the radiation pattern, which indicates fine diversity. Fig. 11(b) shows that the model under consideration has very low element correlations. This shows that there is variety and spatial isolation, which is the best for MIMO system performance. The information in Fig. 11(c) shows substantial spatial diversity and very little signal redundancy.

Two important things make a good MIMO antenna. CCL indicates the extent to which data communication capacity is lost due to signal correlation among multiple antenna ports. For a MIMO antenna to work well, the CCL should be below 0.4 bits/s/Hz. Fig. 11(d) shows that the proposed MIMO MA has a lower CCL, indicating it uses the channels very efficiently. This shows that the antenna performs well in applications requiring high data rates. Table 3 presents the performance of an MTM-based MIMO system compared to the literature.

TABLE 3. Performance comparison of the literature and the presented work.

References	Resonating Frequencies (GHz)	Isolation (dB)	Gain (dBi)	Bandwidth (GHz)
[11]	5.8	−45	6.7	∼0.4
[12]	10.7–12.7	< −20	24.55	2
[13]	5.32–6.35	< −45	3.5	1.03
[14]	1.15–1.49	-	6.17	0.34
[15]	7.025–8.4	< −20	6.4	1.375
[16]	Sub-6	< −15	4.42	4.53
Proposed	28	< −25	14.05	2.1

5. CONCLUSION

In this study, a new, 4-port MIMO antenna with MTM elements operating at 28 GHz in the Ka-band is designed, tested, and validated. The antenna uses a simple patch with U-shaped slots on an FR4 substrate, fed via a microstrip line, with orthogonal alignment to achieve superior isolation. Through a step-by-step design evolution involving feed arrangement optimization, MIMO loaded with MTM superstrate, the proposed antenna achieves isolation levels < -25 dB, reduced ECC (ECC < 0.02), increased diversity gain ($\sim$10 dB), low CCL (CCL < 0.4 bps/Hz), peak gain up to 14.05 dBi, and efficiency up to 95.46%. Compared to existing antennas, this design offers a strong balance between performance and manufacturability. It demonstrates strong potential for integration into high-frequency, multi-port wireless systems, particularly in next-generation communication systems and 5G applications.

REFERENCES

[1] Thomas, S. B., S. Sangeetha, and B. Thomas, "Opportunities and challenges in advanced wireless communication," in *5G and Beyond Wireless Communications*, 13–34, 1st edition, CRC Press, 2024.

[2] Shafik, W., "An overview of computational modeling and simulations in wireless communication systems," in *Computational Modeling and Simulation of Advanced Wireless Communication Systems*, 8–40, 1st edition, CRC Press, 2024.

[3] Yahya, M. S., S. Soeung, S. K. A. Rahim, U. Musa, S. S. B. Hashwan, Z. Yunusa, and S. A. Hamzah, "LoRa microstrip patch antenna: A comprehensive review," *Alexandria Engineering Journal*, Vol. 103, 197–221, 2024.

[4] Yogeshwaran, A., "A multiple resonant microstrip patch heart shape antenna for satellite and Wi-Fi communication," *Analog Integrated Circuits and Signal Processing*, Vol. 121, No. 1, 1–11, 2024.

[5] Karthik Reddy, G., T. Vijetha, G. V. S. M. Kumar, S. Babu, and C. Babaiah, "Antenna optimization using metamaterials," *Journal of Physics: Conference Series*, Vol. 2837, No. 1, 012018, 2024.

[6] Al-Gburi, A. J. A., K. V. Prasad, V. N. K. R. Devana, G. S. Rao, A. Armghan, and A. M. Kassim, "Isolation enhancement in polyimide-based MIMO antennas using slot-based metamaterial defected ground structures and a stub-loaded decoupling network," *Progress In Electromagnetics Research M*, Vol. 137, 66–78, 2026.

[7] Jujjarapu, P. K., N. Suneetha, P. A. Kumar, A. N. Kiran, and B. V. S. Sailaja, "Design of symmetric quad circular radiator antenna with semicircular bridge and DGS for WLAN, ISM band and sub-6 GHz applications," *Progress In Electromagnetics Research C*, Vol. 170, 174–183, 2026.

[8] Ahmad, I., Y. Liu, F. Wang, M. K. Khan, and M. M. Kamal, "Wideband MIMO antenna system with high inter-elements isolation for mm-Wave communications and the Internet of Things (IoT)," *Progress In Electromagnetics Research Letters*, Vol. 124, 37–45, 2025.

[9] Manikonda, R., G. Tamminaina, and S. Gulla, "Design and analysis of high isolation four port MIMO antenna for N77 band 5G communication," *Progress In Electromagnetics Research C*, Vol. 163, 35–42, 2026.

[10] Swetha, A., B. V. S. Rao, B. N. Prasanna, V. N. K. R. Devana, and V. N. S. Doddavarapu, "Simple 8-port 2×2 multiple-input multiple-output patch antenna for reduced complexity and isolation for Ku-band applications," *Physica Scripta*, Vol. 101, No. 21, 215504, 2026.

[11] Elahi, M., S. Koziel, and L. Leifsson, "Self-isolation in MIMO array using mode diversity," *IEEE Access*, Vol. 13, 45 023–45 036, 2025.

[12] Srivastava, G., A. Mohan, S. Kumar, H. C. Choi, and K. W. Kim, "Compact 16-port MIMO antenna for sub-6 GHz communications," *IEEE Access*, Vol. 13, 34 051–34 059, 2025.

[13] Wang, Z.-R., N. Wang, and K.-L. Zhang, "A combined aperture-coupled membrane microstrip patch antenna array," *IET Microwaves, Antennas & Propagation*, Vol. 19, No. 1, e12545, 2025.

[14] Wong, K.-L., S.-E. Hong, and W.-Y. Li, "Low-profile four-port MIMO antenna module based 16-port closely-spaced 2×2 module array for 6G upper mid-band mobile devices," *IEEE Access*, Vol. 11, 110 796–110 808, 2023.

[15] Elabd, R. H. and A. J. A. Al-Gburi, "Ultra-compact 4-port MIMO antenna with defected ground structure and SAR analysis for 28/38 GHz 5G mobile devices," *Journal of Electromagnetic Waves and Applications*, Vol. 38, No. 9, 1000–1025, 2024.

[16] Devana, V. N. K. R., A. K. Sohi, A. Swetha, D. R. Valluri, S. Turpati, Z. Zakaria, and A. J. A. Al-Gburi, "Assessment of a flexible polyimide-based quad-port MIMO antenna for wideband sub-6 GHz 5G applications," *Ain Shams Engineering Journal*, Vol. 17, No. 5, 104044, May 2026.

[17] Ali, A., M. E. Munir, M. M. Nasralla, M. A. Esmail, A. J. A. Al-Gburi, and F. A. Bhatti, "Design process of a compact tri-band MIMO antenna with wideband characteristics for sub-6 GHz, Ku-band, and millimeter-wave applications," *Ain Shams Engineering Journal*, Vol. 15, No. 3, 102579, 2024.

[18] Din, I. U., N. A. Abbasi, W. Ullah, S. Ullah, M. A. Ouameur, and D. N. K. Jayakody, "A novel and compact metamaterial-based four-element MIMO antenna system for millimeter-wave wire-

less applications with enhanced isolation," *International Journal of Antennas and Propagation*, Vol. 2024, No. 1, 7480655, 2024.

[19] Nej, S., S. K. Bairappaka, D. B. D. S. R. Ram, S. Jana, and A. Ghosh, "Design of a high order dual band MIMO antenna with improved isolation and gain for wireless communications," *Arabian Journal for Science and Engineering*, Vol. 50, No. 8, 5727–5744, 2025.

[20] Alrashdan, M. H. S., Z. Al-qudah, and M. A. Bataineh, "Microstrip patch antenna directivity optimization via Taguchi method," *Ain Shams Engineering Journal*, Vol. 15, No. 9, 102923, 2024.

[21] Ghewari, P. and V. Patil, "Advancements in microstrip patch antenna design using nature-inspired metaheuristic optimization algorithms: A systematic review," *Archives of Computational Methods in Engineering*, Vol. 32, No. 6, 3687–3732, 2025.

[22] Rao, N. and D. V. Kumar, "Gain and bandwidth enhancement of a microstrip antenna using partial substrate removal in multiple-layer dielectric substrate," in *Progress In Electromagnetics Research Symposium Proceedings*, 1285–1289, 2011.

[23] Numan, A. B. and M. S. Sharawi, "Extraction of material parameters for metamaterials using a full-wave simulator [education column]," *IEEE Antennas and Propagation Magazine*, Vol. 55, No. 5, 202–211, 2013.